# International Journal of Technology

http://ijtech.eng.ui.ac.id



Research Article

# Numerical Study of STU.1.M Unmanned Aerial Vehicles Stability at the Unsteady State Conditions

Sabah Sameer Almukhtar 1, \*, Mohammed A. Abdulwahid 1, Akeel MA Morad 1

**Abstract:** Unmanned Aerial Vehicle (UAV) is becoming more important across various industries, including agriculture, civil aviation, the military, and the environment. Therefore, this study aimed to investigate the aerodynamic stability of a transient STU.1.M UAV at speed of 40, 60, and 80 m/s with an angle of attack of 6 degrees, corresponding to the lift-to-drag coefficient ratio's maximum value in a steady state. For the numerical analysis, Ansys Fluent was used, while grid-independence evaluation and validity of the numerical solution were conducted by comparing the results of the proposed mathematical model on NACA 0012 airfoil with experimental data using same mathematical model. The results showed that vortices formed and decayed behind aircraft due to flow field's oscillations at specific frequencies. The magnitude of these vortices grew as aircraft speed increased. When the speed increased to 80 m/s, the lift coefficient and lift-to-drag ratio rose by 0.56% and 2.85%, respectively. The lift-to-drag ratio oscillation frequency rose by 102.5%, while the vertical oscillation frequency corresponding to the oscillations of the lift force decreased by 71.7%.

Keywords: Computation fluid dynamic; Drag; Frequency; Lift; Unmanned aerial vehicles

# 1. Introduction

Unmanned Aerial Vehicle (UAV) is autonomous aircraft operating without human pilots directing flight controls (Dickes et al., 2000). Because UAV has the potential to benefit aircraft industry, several investigations are being carried out continuously. The associated benefits include being less costly compared to conventional jet aircraft, the elimination of risk to human pilots, ability to fly autonomously for longer periods of time in hazardous regions (Boelens, 2012). The motion as well as interaction of air around and with solid objects have gained significant attention in the subfield of fluid dynamics known as aerodynamics. When objects move in air at limited speed and the Mach number does not exceed 0.3, the density changes are small and the flow is called incompressible fluid flow. The changes in forces and momentum are linear, and this science is called linear aerodynamics (Klein and Morelli, 2006). In contemporary engineering, time-varying fluid flow alongside unsteady aerodynamic forces and moments are increasingly relevant, particularly when vehicle experiences turbulence. Therefore, cars, boats, and aircraft are designed with high optimization to streamline the body and increase efficiency by reducing drag and flow separation (Kubo, 2006).

Molaa and Abdulwahid (2024) conducted a numerical and experimental study of the significant impact on the aerodynamic properties of the NACA0012 airfoil. The results showed remarkable agreement between the numerical modeling and practical tests, contributing to a better understanding of the airfoil performance under turbulent conditions. Song et al. (2023) comprehensively reviewed mission planning methods for UAV fleets, categorizing different

<sup>&</sup>lt;sup>1</sup>Department of Thermal Mechanics Engineering Technical Engineering College/Basra, Southern technical university, Basra, 61001, Iraq

<sup>\*</sup>Corresponding author: Sabah.s.almukhtar@fgs.stu.edu.iq; Tel.: +9647827932232

strategies based on operational environments, which showed technical challenges and future trends in this field. Furthermore, Zhang et al. (2024) conducted an experimental and numerical study on the secondary flow system of a supersonic aircraft wing using a wind tunnel to simulate actual flight conditions. The results showed good agreement between the numerical simulation and tests, which contributed to the improvement of supersonic wing design.

Dastjerdi et al. (2021) presented an innovative design for vertical-axis wind turbines using a simultaneous combination of symmetric and curved airfoils. The results showed high aerodynamic performance compared to conventional designs, enhancing the potential of turbines in diverse environments. Furthermore, Majid and Jo (2021) conducted a comparative study between the aerodynamic performance of conventional and camber morphing airfoils. Based on the results, camber morphing airfoils showed high performance in terms of lift and aerodynamic efficiency, indicating their potential in advanced aviation applications. Somashekar and Raj (2021) carried out a comparative study to evaluate the accuracy of different turbulence models in predicting the aerodynamic properties of small UVA. The results showed that the performance of the models varied in representing the airflow, which helped in selecting the most appropriate model to improve the simulation accuracy. Mubassira et al. (2021) also performed a numerical study of the characteristics of the NACA 4312 airfoil when a Gurney slat was added. The results showed a significant improvement in lift force without a significant increase in drag force, indicating the effectiveness of the slat in improving the aerodynamic performance of airfoils.

The potential of unsteady aerodynamics for engineering design is best shown by biological propulsion. Previous studies have reported that fish, insects, birds, and bats frequently use unsteady fluid dynamics to enhance the maneuverability, maximize thrust and lift, causing an improvement propulsive efficiency (Roy et al., 2007). Unsteady aerodynamic forces are becoming more significant during agile maneuvers and gust disturbances as UAV gets lighter and smaller. Over the past century, the need for precise, effective aerodynamic models has served as a major driving force for several investigations. To design aircraft and assess aeroelastic as well as flight dynamic stability, aerodynamic models are essential tools (Selig, 2010).

The quasi-steady assumption is the foundation of the majority of aerodynamic models used for flight control. This assumption states that forces and moments depend statically on parameters like relative velocity and angle of attack. However, the unsteady aerodynamic forces necessary for small and agile aircraft to avoid obstacles, react to gusts, and track potentially elusive targets are not described by the models (Leishman, 2006; Schlichting and Truckenbrodt, 1979). Despite the limitations, the literature contains a large number of unsteady aerodynamic models. These include the classical unsteady models of Theodorsen (Hodges and Pierce, 2011; Wagner 2006), which continue to serve as a standard for other linear models. By convolving the motion's time derivative with the analytically calculated step response, Wagner's model generates the lift in response to arbitrary input motion. Theodorsen used the same assumptions of an incompressible, inviscid, planar wake to create an analogous model in the frequency domain. With the resources available at the time, model developed by Theodorsen was considered appropriate for the analysis of flutter instability, although restricted to sinusoidal input motion. Direct numerical simulations (DNS) (Taira and Colonius, 2009a; Williams et al. 2008), computational fluid dynamics (CFD) (Salmon and Chatellier, 2022; Ronch et al., 2012; Amsallem et al. 2010; Taira and Colonius, 2009b; Murman, 2007; Sitaraman and Baeder 2004), wind tunnel experiments (Williams et al. 2008; Pelletier and Mueller, 2000), and water channel experiments (Buchholz and Smits 2008; Fransos and Bruno 2006) can all be used to create sophisticated models for the unsteady fluid dynamics and aerodynamic forces. The viscous fluid dynamic interactions causing transient unsteady aerodynamics may be accurately estimated using any of these methods. However, the application is very costly in terms of both time and equipment, showing the need to extract low-dimensional models from intricate model system such as UAV (Swischuk et al., 2020; Green and Smits 2008; Gold and Karpel 2008; Ol et al., 2005; Mor and Livne 2005; Silva and Bartels, 2004).

A model for a small fixed-wing UAV at high angles of attack has been developed by (Johnson and Lind, 2009), based on flight test data. By using least squares regression curve fitting, transfer functions are identified from aileron, elevator, and rudder commands to roll, pitch, and yaw rates. In a related application, (Green and Oh, 2009; 2005) presented a controller for the hover maneuver of a small fixed-wing manned aerial vehicle (MAV). Since nonlinear or unsteady aerodynamics are not included, controller's dynamics are modeled using first principles and simplified.

Kaplan et al. (2007) explored the effect of Reynolds number and aspect ratio on small wings. These factors become increasingly important for larger amplitude maneuvers at high angles of attack. Under the conditions, nonlinear separated flow effects like vortex shedding (Leishman et al., 2002) and dynamic stall (Zhang and Graham, 2020). are crucial and must be modeled to ensure stable as well as responsible flight. In addressing performance challenges under these unsteady conditions, materials like Polyethylene Terephthalate (PET) offer promising solutions. Patel et al. (2023) showed that PET could enhance structural robustness, critical for UAV stability in dynamic environments. For instance, STU.1.M UAV must maintain reliable operation under turbulent atmospheric conditions while also navigating broader challenges related to economic disruptions and climate change, significantly impacted food and medical supply chains (Sharma et al., 2024).

This study is a continuation of the investigation into aerodynamic stability of flow through the STU.1.M UAV. In previous reports, the changes in CL, CD, and CL/CD values were explored over the entire aircraft body under steady state conditions as the angle of attack. The results showed that the optimum angle to achieve maximum CL/CD was 6 degrees. Therefore, this study aimed to explore the behavior and aerodynamic stability at 6 degrees in the unsteady state using numerical modeling at 40, 60, and 80 m/sec aircraft velocity. The analysis was carried out to evaluate the aerodynamic performance of STU.1.M UAV from the fluctuation of flow field caused by the passage through aircraft body.

# 2. Materials and Methods

Flow-induced vibration (FIV) is defined as the mechanical vibration of structures within a fluid flow or fluid carrier (such as pipes). Many engineering structures are subject to the interaction between aerodynamic and inertial forces, including damping and elasticity of structures (Bernitsas et al., 2008). This phenomenon is essential in non-streamlined structures, which are more susceptible because of exposure to boundary layer separation. Generally, aerodynamic forces that affect aircraft body in flow are caused by two factors. These include the distribution of pressure and the shear stress resulting from viscosity on the immersed surface of the body. Pressure affects the body tangentially, causing lift, while shear stress influences the surface of the body tangentially, causing drag (Bibo and Daqaq, 2015). Under certain conditions, these forces cause the body to move, thereby affecting the position relative to the flow, leading to a change in the aerodynamic forces and the occurrence of a vibration phenomenon (Salmon and Chatellier, 2022).

In this study, the lift and drag coefficient values affecting the STU.1.M UAV were determined using unsteady CFD numerical modeling, and the following relationships were identified (Salmon and Chatellier, 2022):

$$C_L = \frac{F_L}{0.5\rho V^2 A}$$
 ,  $C_D = \frac{F_D}{0.5\rho V^2 A}$  (1)

where A is the area of the UAV projection on a plane perpendicular to the flow direction (m²), V is the UAV speed (m/sec), and FL and FD stand for lift and drag force (N), respectively, and  $\rho$  is air density (Kg/m³) (Salmon and Chatellier, 2022). The numerical solution was carried out using Ansys Fluent. SolidWorks was used to draw the UAV model and the surrounding fluid domain, and Ansys meshing was used to create the mesh. The mesh was then exported to Fluent for the numerical solution. A 3970 x 32 core AMD thread ripper computer with 128 GB of DDR5 RAM was utilized.

The drawing of STU.1.M UAV model and creating fluid domain around were the first stages of numerical modelling. SolidWorks software was used to draw aircraft model in the actual

dimensions. A diagram of the drawn UAV is shown in Figure 1, and the characteristic values are presented in Table 1.

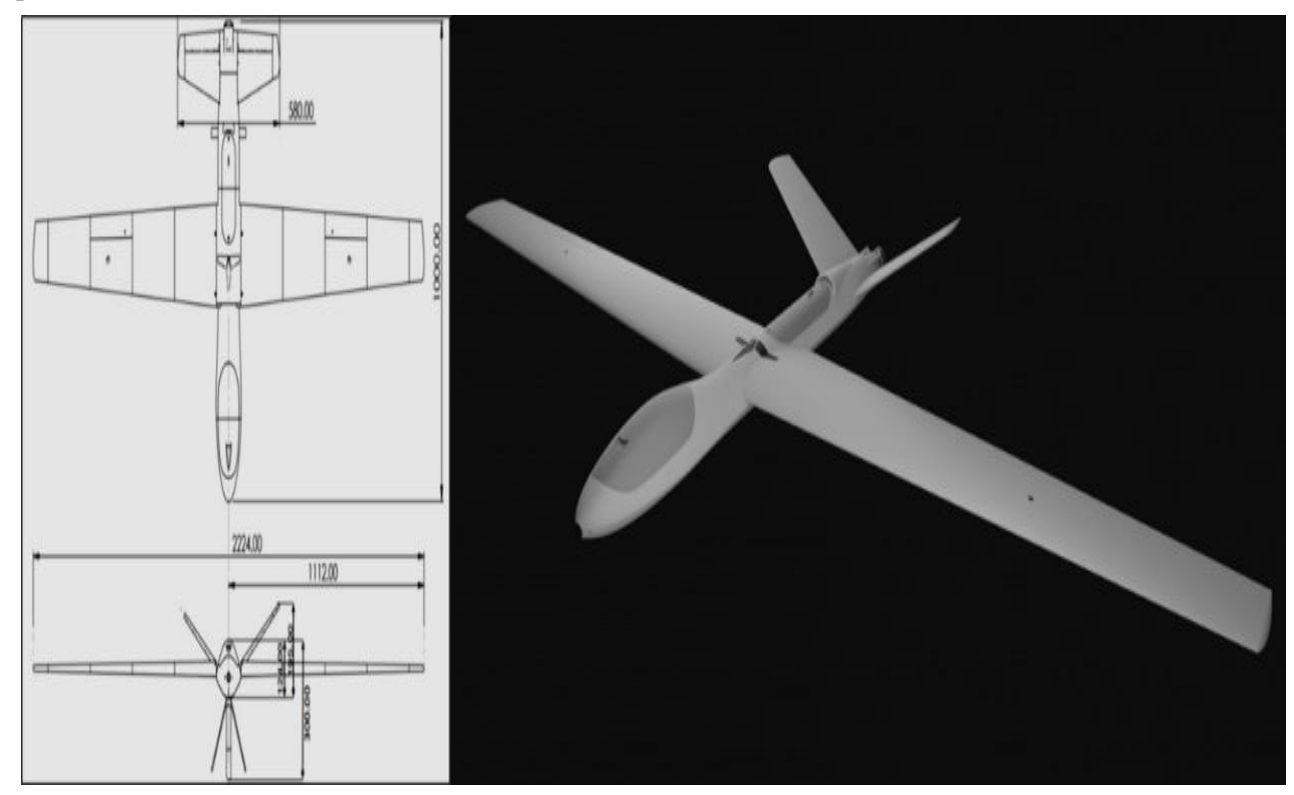


Figure 1 Main dimensions of STU.1.M UAV

**Table 1** Designed parameters of STU.1.M UAV

No.	Dimensions	The symbol	Value
1	Wing length	L	105 cm
2	Wing span	b	224 cm
3	Root chord	cr	29 cm
4	Tip chord	ct	12.4 cm
5	Aspect ratio	AR	12.9
6	Taper ratio	λ	0.42
7	Wing area	A	4636.8 cm <sup>2</sup>
8	Dihedral	D	0
9	Sweep	S	0
10	Chord line	c	20.7cm

Taper type wing NACA 2410 is used and the tail is a V-type

In order to minimize flow distortion, domain type C was used in this study to reduce mesh and expedite the solution process. The plane location was five times the chord length upstream and 10 times downstream. Specifically, the domain comprised four faces, including the wing and inlet side have an area of 1.2397 m<sup>2</sup>, the outlet covers  $102.02 \text{ m}^2$ , and the inlet is  $298.94 \text{ m}^2$ . Figure 2 shows the bounding box (length x = 4.379 m, length y = 23.296 m, length z = 29.813 m).

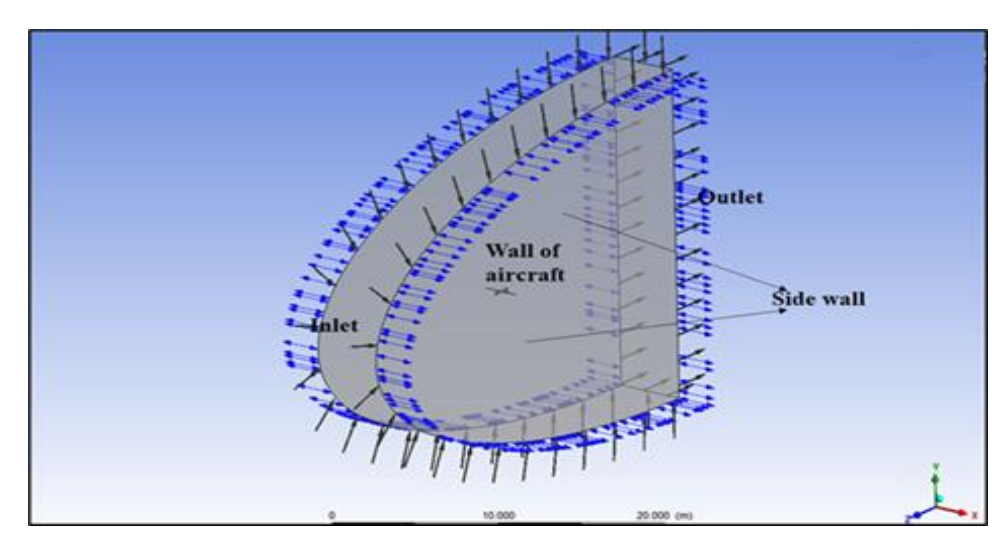


Figure 2 Fluid Domain and Boundary Conditions

#### 2.1. Mathematical model

Computational fluid dynamics (CFD) was used to model fluid flow. This tool has been used by several commercial software programs to analyze engineering systems, solve problems, and show the results. Solving this problem numerically included evaluating a set of differential equations describing the movement. These equations included the continuity and the momentum equations, which were given by the following relationships (Andersson et al., 2012):

$$\frac{\partial \rho}{\partial t} + \frac{\partial (\rho u)}{\partial x} + \frac{\partial (\rho v)}{\partial y} + \frac{\partial (\rho w)}{\partial z} = 0 \tag{2}$$

The continuity equation expresses the law of conservation of mass within the control volume under consideration, stating that the net time rate of mass entering and leaving must equal the change in mass within the control volume with time.  $\rho$  is the Fluid density, u,v and w is the velocity components on the x, y, and z directions. Momentum equations in X, Y, and Z directions are as follows (Chaoqun et al., 2018):

$$\rho(\frac{\partial u}{\partial t} + u \frac{\partial u}{\partial x} + v \frac{\partial u}{\partial y} + w \frac{\partial u}{\partial z}) = -\frac{\partial p}{\partial x} + \rho g_x + \mu(\frac{\partial^2 u}{\partial x^2} + \frac{\partial^2 u}{\partial y^2} + \frac{\partial^2 u}{\partial z^2})$$
(3)  

$$\rho(\frac{\partial v}{\partial t} + u \frac{\partial v}{\partial x} + v \frac{\partial v}{\partial y} + w \frac{\partial v}{\partial z}) = -\frac{\partial p}{\partial y} + \rho g_y + \mu(\frac{\partial^2 v}{\partial x^2} + \frac{\partial^2 v}{\partial y^2} + \frac{\partial^2 v}{\partial z^2})$$
(4)  

$$\rho(\frac{\partial w}{\partial t} + u \frac{\partial w}{\partial x} + v \frac{\partial w}{\partial y} + w \frac{\partial w}{\partial z}) = -\frac{\partial p}{\partial z} + \rho g_z + \mu(\frac{\partial^2 w}{\partial x^2} + \frac{\partial^2 w}{\partial y^2} + \frac{\partial^2 w}{\partial z^2})$$
(5)

$$\rho(\frac{\partial v}{\partial t} + u\frac{\partial v}{\partial x} + v\frac{\partial v}{\partial y} + w\frac{\partial v}{\partial z}) = -\frac{\partial p}{\partial y} + \rho g_y + \mu(\frac{\partial^2 v}{\partial x^2} + \frac{\partial^2 v}{\partial y^2} + \frac{\partial^2 v}{\partial z^2})$$
(4)

$$\rho(\frac{\partial w}{\partial t} + u\frac{\partial w}{\partial x} + v\frac{\partial w}{\partial y} + w\frac{\partial w}{\partial z}) = -\frac{\partial p}{\partial z} + \rho g_z + \mu(\frac{\partial^2 w}{\partial x^2} + \frac{\partial^2 w}{\partial y^2} + \frac{\partial^2 w}{\partial z^2})$$
 (5)

The conservation of momentum equation expresses Newton's second law, stating that the sum of the external forces acting on the control volume is equal to the inertial forces. The primary external forces acting on aircraft are viscous forces, pressure, and gravity. Moreover, lift and drag forces are generated from viscous and pressure forces. P is pressure (Pa),  $\,^{\mu}$  is viscosity (Pa.sec), g is acceleration due to gravity (m/sec<sup>2</sup>),  $\rho$  and density (Kg/m<sup>3</sup>), and (u, v, and w) are the velocity components on the x, y, and z directions (m/sec), respectively.

In comparison, turbulence model  $k\omega$  – SST is considered more stable and dependable than the k-omega turbulence model because it uses the k-epsilon equations outside of the boundary layer region and the normal k-omega equations inside. This allows for more accuracy close to the boundary layer region wall. With the addition of a term  $D_{\omega}$  pertaining to the frequency dissipation of the turbulence within the  $^{\emptyset}$  equation's bounds, the K-omega-SST is comparable to the K-omega turbulence model (Chaogun et al., 2018).

$$\frac{\partial(\rho\omega)}{\partial t} + \frac{\partial(\rho\omega u_j)}{\partial x_j} = \alpha \frac{\omega}{k} \tau_{ij} \frac{\partial u_i}{\partial x_j} - \gamma \rho \omega^2 + \frac{\partial}{\partial x_j} \left[ (\mu + \sigma_{22}\mu_t) \frac{\partial \omega}{\partial x_j} \right] + D_{\omega}$$
 (6)

Whereas

$$D_{\omega} = 2(1 - F_1) \frac{\rho}{\omega \sigma_{\omega 2}} \frac{\partial k}{\partial x_i} \frac{\partial \omega}{\partial x_i} \tag{7}$$

$$F_1 = \tanh(\phi_1^4) \tag{8}$$

$$\phi_1 = min[max(\frac{\sqrt{k}}{0.09\omega y}, \frac{500\mu}{\rho y^2 \omega}), \frac{4\rho k}{\sigma_{\omega 2} D_{\omega}^{+} y^2}]$$
(9)

$$D_{\omega} = 2(1 - F_{1}) \frac{\rho}{\omega \sigma_{\omega 2}} \frac{\partial k}{\partial x_{j}} \frac{\partial \omega}{\partial x_{j}}$$
(7)  

$$F_{1} = tanh(\phi_{1}^{4})$$
(8)  

$$\phi_{1} = min[max(\frac{\sqrt{k}}{0.09\omega y}, \frac{500\mu}{\rho y^{2}\omega}), \frac{4\rho k}{\sigma_{\omega,2} D_{\omega}^{+} y^{2}}]$$
(9)  

$$D_{\omega}^{+} = max[2 \frac{\rho}{\omega \sigma_{\omega 2}} \frac{\partial k}{\partial x_{j}} \frac{\partial \omega}{\partial x_{j}}, 10^{-10}]$$
(10)

where  $\tau_{ij}$  represents the shear stress resulting from viscosity,  $\mu_t$  is vortex viscosity, and  $\mu_t$  is kinematic viscosity. Table 2 shows the values of the constants in the previous equations (Zhao and Su, 2018):

Table 2 Constant Values of K-Omega SST Turbulence Model

$\sigma_{\scriptscriptstyle \omega 2}$	$\sigma_{\scriptscriptstyle{22}}$	$\sigma_{\!\scriptscriptstyle 11}$	β	γ	α
1.168	1/2	1/2	9/100	3/40	5/9

# 2.2. Assumptions and boundary conditions

There is a need to establish suitable boundary conditions in order to solve the previous mathematical model. These boundary conditions are shown in Figure 2 and Table 3.

**Table 3** Boundary Conditions

<u></u>	
Velocity Inlet (Components)	Inlet
Pressure Outlet (Zero Atmospheric Gage Pressure)	Outlet
No Slip Condition	Wall Of Aircraft
Symmetry	Side Wall

The flow could be regarded as incompressible for angles of attack (0, 2, 4, 6, 8, 10, 12, and 14 degrees). This was because the velocity values selected (20, 40, 60, and 80 m/sec) were all at Mach numbers less than 0.3, then Physical properties of air at these conditions are indicated in Table 4. The study was carried out in three dimensions and a transient state with fixed air property values.

**Table 4** Physical Properties of Air

Viscosity (Pa.s)	$1.7894x10^{-5}$
density $\int_{0}^{\infty} (Kg/m^3)$	1.225

#### 2.3. Meshing of domain

A fundamental factor ensuring the validity of the numerical solution is the mesh generation procedure. In order to guarantee the modeling of the viscous sublayer regime within the boundary layer, the mesh is refined by testing the value of Y+ at the walls until it is extremely small (Y+<1) [39].

As shown in Figure 3, tetrahedral mesh was generated using Ansys meshing (left of Fig S1) and converted to polyhedral mesh in Ansys Fluent (right of Fig S1). This ensured a reduction in the number of element accounts, thereby decreasing computational cost. In this study, tetrahedral mesh of five different sizes (3743532, 7742139, 9549582,13040520, and 14200000) was examined. The CL/CD value at 80 m/Sec velocity was selected to monitor the variation with respect to number of cells, as shown in Figure S2. As shown in Figure 4, the value of CL/CD quantity remained constant at value of 8.96 when the number of cells reached 13 million or more. Therefore, the cell count was selected for numerical simulation to ensure both accuracy and computational efficiency.

#### 2.4. Results Validation

Due to the lack of experimental results for STU.1.M UAV and the accuracy of the numerical results was verified. The proposed physical model was tested with the same boundary conditions on the benchmark motion of a NACA 0012 airfoil at 1000 Reynolds number when air moved over and started to vibrate. This case was similar to the vibration from the movement of aircraft in the air. Figure 5 shows the modeling of NACA 0012 airfoil in reference (Kurtulus, 2019) which contains experimental results using the same mathematical model and boundary conditions in this study.

In the study by (Kurtulus, 2019), the flow vibration around NACA 0012 at Reynolds number was explored and the numerical results were compared with the experimental data. Figures (3-a) and (3-b) state the domain and mesh boundary layer, while Figures (3-c) and (3-d) show vorticity and velocity contours for the wing at 10 degrees angle of attack and Re=1000, alongside value of the instantaneous lift coefficient and spectrum frequency at the same angle of attack. Table 5 shows a comparison of the experimental data with the numerical results calculated at the same angle of attack.

Table 5 Validate the Numerical Simulation

	CL Average	CD Average	f (Hz)
Reference [41]	0.56	0.19	4.4
Current study	0.54	0.18	4.68
Percentage error %	3.57%	5.26%	6.36%

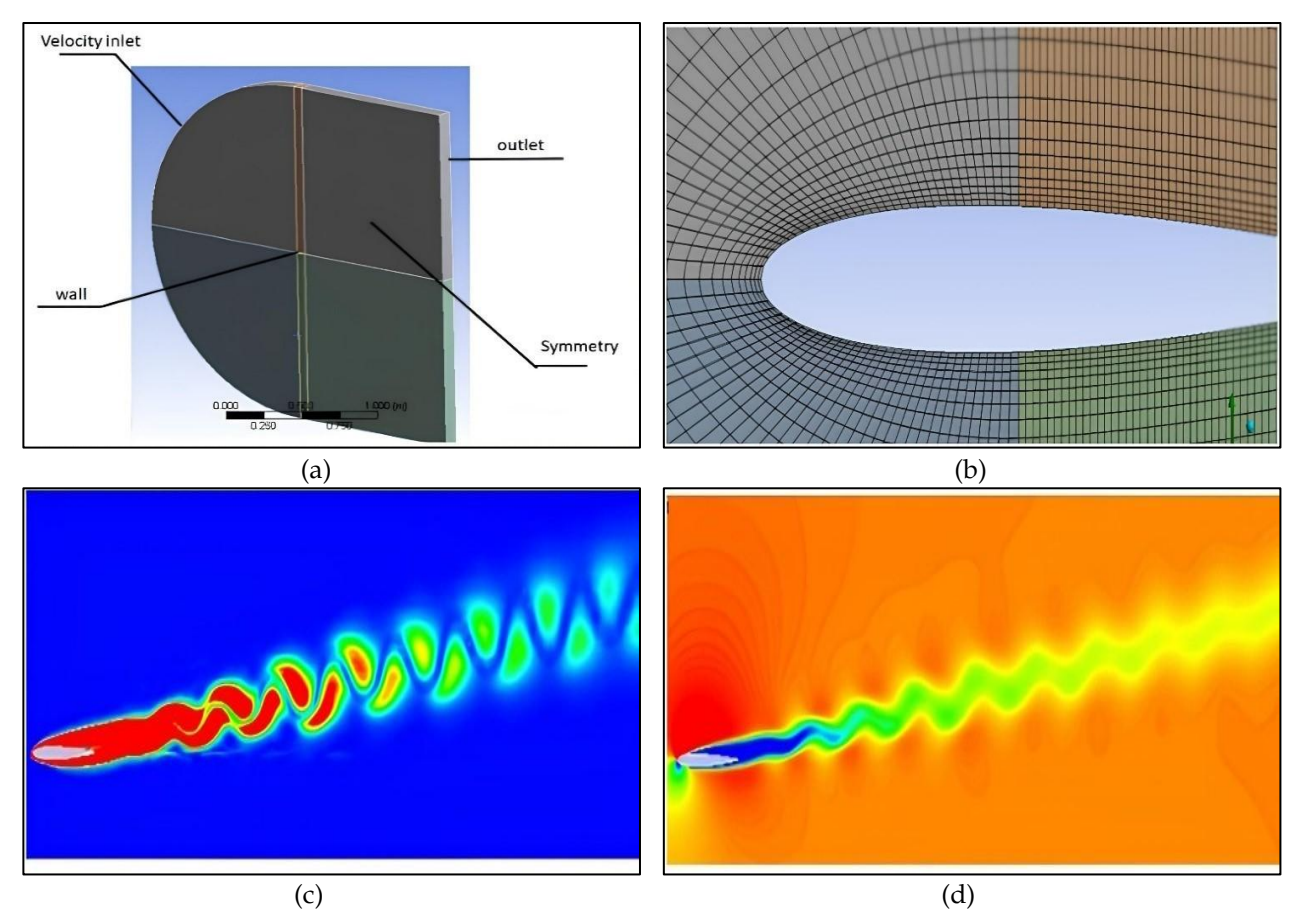


Figure 3 (a) Domain type C (b) Mesh boundary layer (c) Vorticities contours (d) Velocity contours

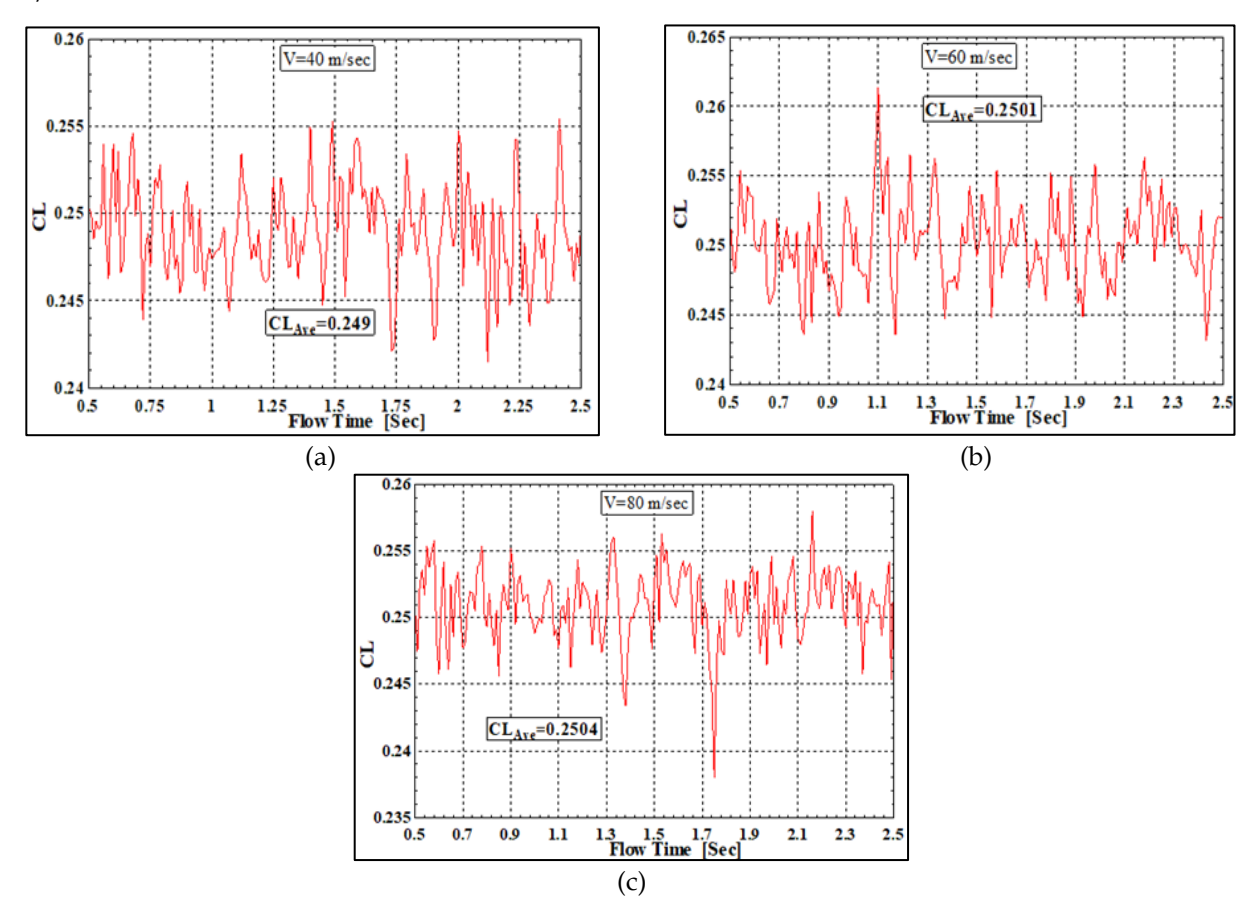
The average lift and drag values for different angles of attack are shown in Figure S4, and a comparison of these results with experimental results (Kurtulus, 2019). Table 5 shows a clear agreement between the numerical results and experimental data. This suggests that the

mathematical model and numerical modeling used in this study show results with acceptable accuracy. Kurtulus (2019) explored a 2D or planar model and observed that flow field did not change with 3D effects. However, the validation model used in this study was 3D with a small thickness to reduce the computational cost. Despite being 3D, this model produced results equivalent to 2D when the cross-sectional area was matched between the two models. The analysis was performed in 3D to represent the actual geometry of UAV.

#### 3. Results and Discussion

In order to solve the required mass conservation, momentum, and turbulence equations in unsteady state, a simple algorithm was selected as a method for velocity-pressure coupling. A 0.0001 sec time step size during 2.5 sec of flow time was used, which required 25000-time steps. The lift and drag coefficients were monitored, and the mass conservation equation residuals were adjusted. Meanwhile, the rest of the equations were allowed to converge under appropriate tolerance. Second-order discretization was selected for all equations to enhance accuracy.

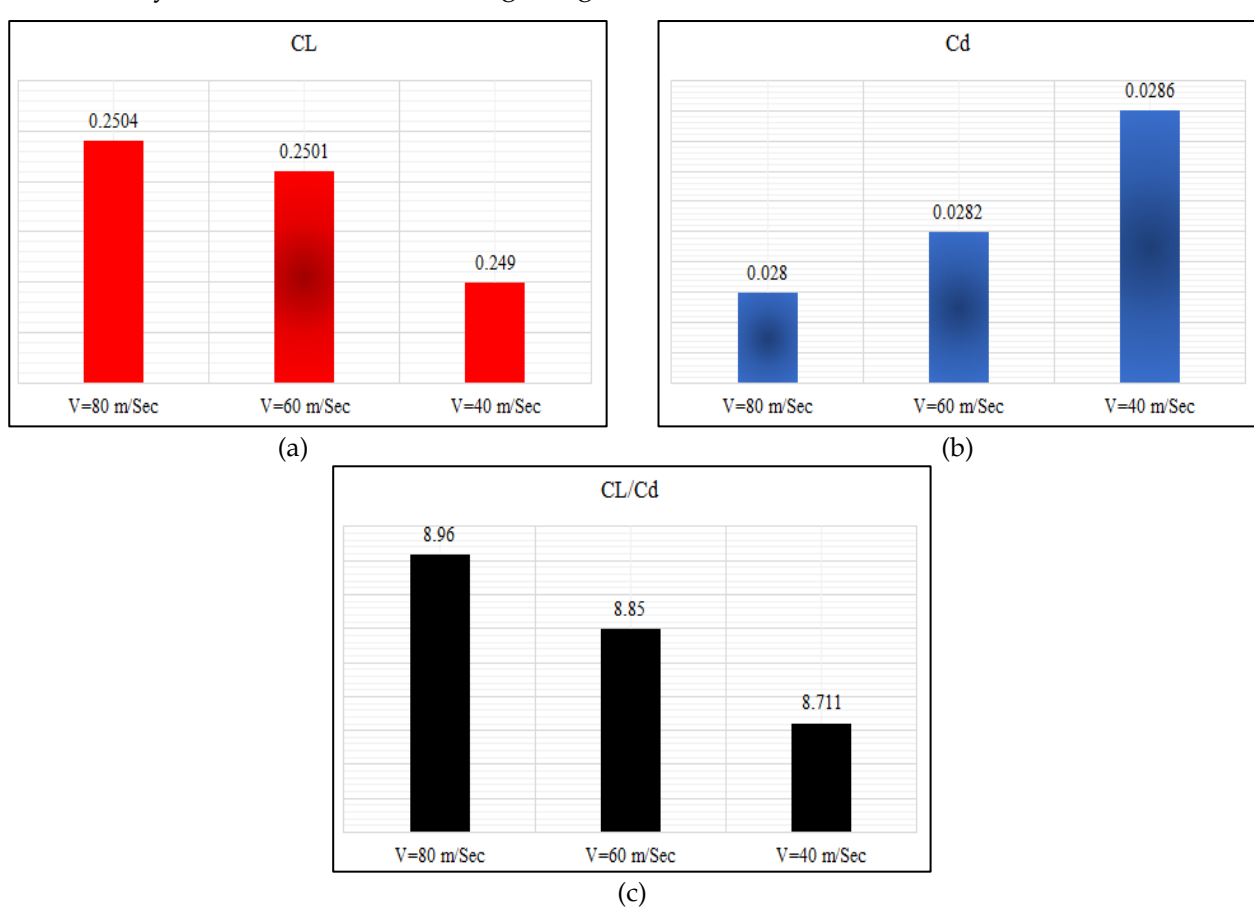
The pressure and velocity contours around the fuselage are shown in Figures S5 and S6. These contours showed the stagnation points at the front of aircraft where the speed value was zero with maximum pressure. Compared to steady-state pressure and speed contours, the formation of vortex separation regions was observed behind aircraft. These regions were not identified when studying flow through the fuselage in steady state. The vortices form and separate at a specific frequency and are extremely small to be directly observed from pressure contours at low speeds. However, at high speeds (80 m/s), vortices started to appear in the speed and velocity contours, as shown in Figures S5 and S6. This can be explained by discussing the graphs showing the changes in the lift and drag coefficients, as well as the lift-to-drag ratio in Figures S7/S8 for the Transient Signal of CL/CD Coefficient.



**Figure 4** (a) Transient Signal of CL Coefficient at V=40m/sec (b) Transient Signal of CL Coefficient at V=60m/sec (c)Transient Signal of CL Coefficient at V=80m/sec

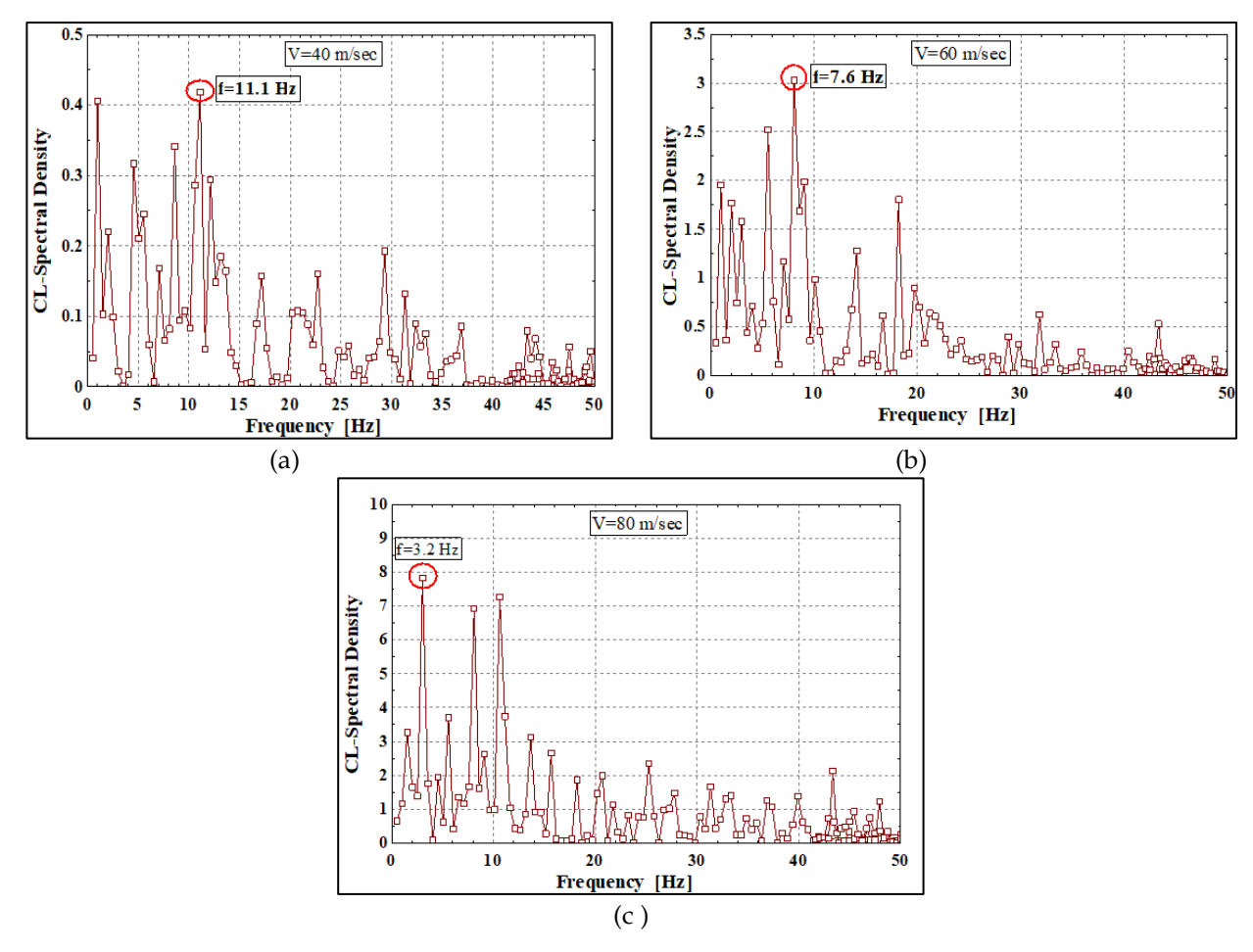
Figures (4-a), (4-b) and (4-c) display the time-varying nature of the CL Coefficient, indicating the presence of vortices from the oscillating flow behind aircraft. Figures (5-a), (5-b) and (5-c) illustration the average values of the drag as well as lift coefficient and the lift-to-drag ratio at each speed. These values are equal to coefficient obtained in steady state. Furthermore, the value of the lift coefficient and the lift-to-drag ratio increase slightly with rising flow velocity. The lift coefficient increases by 0.56% from a value of 0.249 to 0.2504 at a speed of 40 m/sec and 80 m/sec, respectively. Meanwhile, the lift-to-drag ratio increases by 2.85% from 8.711 to 8.96 at a speed of 40 m/sec and 80 m/sec. The change in drag coefficient in the range of speed observed is negligible due to the small value of drag forces on aircraft.

Figure (5-a) states the deviation of the lift coefficient value from the average value increases from 0.65% to 1% at a speed of 40 m/sec and 80 m/sec, respectively. Figure (5-b) shows the deviation of the drag coefficient value increases from 10.5% to 16.1% at a speed of 40 m/sec and 80 m/sec, respectively. Figure (5-b) demonstrates the ratio of the lift coefficient to the drag coefficient increases from 31% at a speed of 40 m/sec to 36.6% at a speed of 80 m/sec. This shows the vortices seen behind aircraft at a high speed of 80 m/sec. To assess the severity of fluctuations from flow field, there is a need to calculate the dominant flow frequency and compare with the natural frequency of aircraft body to avoid resonance during design.



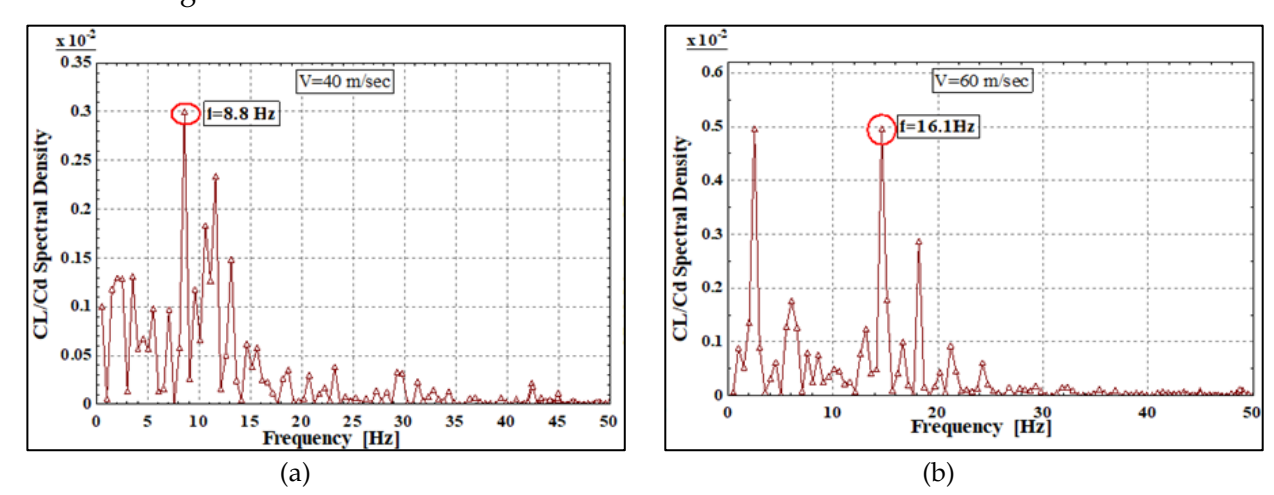
**Figure 5** (a) Average values of CL coefficient (b) Average values of CD coefficient (c) Average Values of CL/CD ratio

By performing a Fast Fourier Transform analysis of the above signals, the dominant frequency of the oscillations of both the lift coefficient and the lift-to-drag ratio can be calculated. However, this study did not analyze the drag coefficient change signal that was integrated within the lift-to-drag ratio signal. Figures (6-a), (6-b) and (6-c) show a Fast Fourier Transformer analysis of the oscillation signal of the lift coefficient.

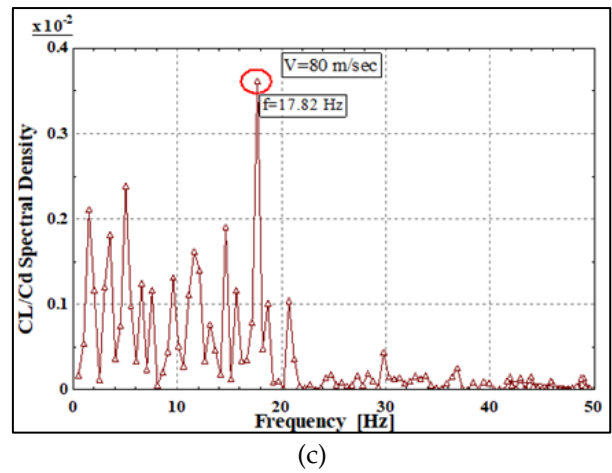


**Figure 6** (a) Fast Fourier Transform of CL signal at V=40m/sec (b) Fast Fourier Transform of CL signal at V=60m/sec (c) Fast Fourier Transform of CL signal at V=80m/sec

Figures (7-a), (7-b) and (7-c) show a Fast Fourier Transformer analysis of the oscillation signal of the lift-to-drag coefficient ratio.

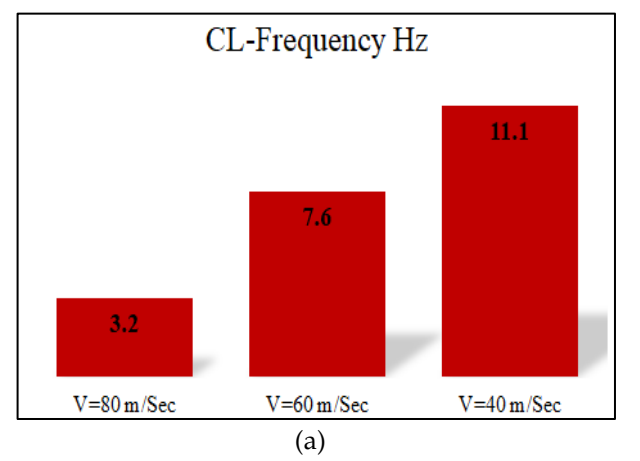


**Figure 7** (a) Fast Fourier Transform of CL/CD signal at V=40m/sec (b) Fast Fourier Transform of CL/CD signal at V=60m/sec (c) Fast Fourier Transform of CL/CD signal at V=80m/sec



**Figure 7** (a) Fast Fourier Transform of CL/CD signal at V=40m/sec (b) Fast Fourier Transform of CL/CD signal at V=60m/sec (c) Fast Fourier Transform of CL/CD signal at V=80m/sec (Cont.)

Figures (8-a) and (8-b) show the CL and CL/CD dominant frequency value at each speed. Based on the results, the dominant frequency of lift oscillations decreased from 11.1 Hz to 3.2 Hz at 40 m/sec and 80 m/sec, respectively, indicating a 71.7% reduction. The frequency of lift-to-drag coefficient oscillations increased from 8.8 Hz to 17.82 Hz (102.5%) at 40 m/sec and 80 m/sec. This is due to the small changes in the drag coefficient.



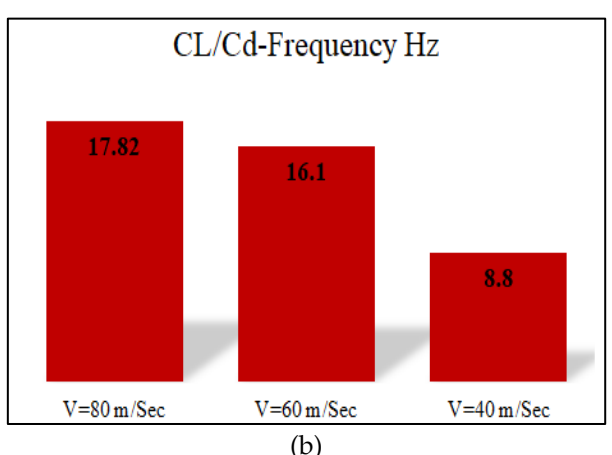


Figure 8 (a) Values of CL signal dominant frequency (b) Values of CL/CD signal dominant frequency

The large changes in the lift oscillation frequency and the low drag coefficient at high speeds in this study explain the pronounced appearance of vortices. Moreover, future studies should explore materials to reduce fouling effects on UAV surfaces, similar to the solutions proposed for boiler chimneys (Kakade et al., 2023). The integrations could stabilize unsteady state performance in extreme environments. Further studies need to explore specialized UAV applications for food supply chains, building on the identified needs of traditional markets like Raipur's fish distribution system (Punekar et al., 2023). Finally, there is a need to consider integrating health and environmental critiques, as stated by Kumar et al. (2024), who discusses that exposure to drone emissions or signal interference correlates with broader concerns.

# 4. Conclusions

In conclusion, this study explores aerodynamic of UAV in unsteady state. Numerical simulations are conducted using Ansys Fluent at flow speeds of 40, 60, and 80 m/s at an angle of attack of 6 degrees, corresponding to the maximum value of the lift-to-drag coefficient ratio in steady state.

The grid-independence study is also performed and the validity of the numerical solution is verified by comparing the results of the proposed mathematical model on NACA 0012 airfoil with experimental data to confirm the validity of the mathematical model. The results of the numerical simulations indicate formation and decay of vortices behind aircraft show that the magnitude of these vortices increases with rising aircraft speed. Additionally, the lift coefficient increases by 0.56%, and the lift-to-drag ratio rises by 2.85% when aircraft speed reaches 80 m/s. The frequency of oscillation of the lift-to-drag ratio also increases by 102.5%. The vertical oscillation frequency corresponding to the oscillation of the lift force decreases by 71.7%. The statistical study of the standard deviation of the lift and drag coefficient as well as the lift-to-drag ratio from the average value also shows an increase in deviations with the rise in aircraft speed. In line with the analysis, the standard deviation of the lift forces increases by 0.65%. Meanwhile, drag forces and the lift-to-drag ratio increase by 10.5% and 36.6%, respectively, when aircraft speed rises from 40 m/s to 80 m/s.

# Acknowledgements

The authors are grateful to the members of the study team, Mohammed A. Abdulwahid and Akeel MA Morad, for their invaluable contributions and collaboration.

## **Author Contributions**

Sabah S. Almukhtar: Conceptualization, Methodology, Data curation, Writing- Original draft preparation. Mohammed A. Abdulwahid: Investigation and Supervision. Akeel MA Morad: Writing- Reviewing and Editing,

#### **Conflict of Interest**

The authors declare no conflicts of interest.

# Research Funding

This research receives no funding.

#### References

Amsallem, D, Cortial, J & Farhat, C 2010, 'Towards real-time computational-fluid-dynamics-based aeroelastic computations using a database of reduced-order information', *AIAA Journal*, vol. 48, no. 9, pp. 2029–2037, <a href="https://doi.org/10.2514/1.j050233">https://doi.org/10.2514/1.j050233</a>

Andersson, B, Andersson, R, Håkansson, L, Mortensen, M, Sudiyo, R, & Van Wachem, B 2012, *Computational fluid dynamics for engineers*, Cambridge University Press, https://doi.org/10.1017/cbo9781139093590

Bernitsas, MM, Raghavan, K, Ben-Simon, Y & Garcia, EMH 2008, 'VIVACE (Vortex Induced Vibration Aquatic Clean Energy): A new concept in generation of clean and renewable energy from fluid flow', *Journal of Offshore Mechanics and Arctic Engineering*, vol. 130, no. 4, article 041101, <a href="https://doi.org/10.1115/1.2957913">https://doi.org/10.1115/1.2957913</a>

Bibo, A & Daqaq, MF 2015, 'An analytical framework for the design and comparative analysis of galloping energy harvesters under quasi-steady aerodynamics', *Smart Materials and Structures*, vol. 24, no. 9, article 094006, <a href="https://doi.org/10.1088/0964-1726/24/9/094006">https://doi.org/10.1088/0964-1726/24/9/094006</a>

Boelens, OJ 2012, 'CFD analysis of the flow around the X-31 aircraft at high angle of attack', *Aerospace Science and Technology*, vol. 20, no. 1, pp. 38–51, <a href="https://doi.org/10.1016/j.ast.2012.03.003">https://doi.org/10.1016/j.ast.2012.03.003</a>

Buchholz, JHJ & Smits, AJ 2008, 'The wake structure and thrust performance of a rigid low-aspect-ratio pitching panel', *Journal of Fluid Mechanics*, vol. 603, pp. 331–365, https://doi.org/10.1017/s0022112008000906

Chaoqun, L, Jiyuan, T & Ghorashi, G 2018, *Computational fluid dynamics: A practical approach*, Elsevier Inc

Dastjerdi, SM, Gharali, K, Al-Haq, A & Nathwani, J 2021, 'Application of simultaneous symmetric and cambered airfoils in novel vertical axis wind turbines', *Applied Sciences*, vol. 11, no. 17, article 8011, <a href="https://doi.org/10.3390/app11178011">https://doi.org/10.3390/app11178011</a>

Dickes, E, Ralston, J & Lawson, K 2000, 'Application of large-angle data for flight simulation', *Modeling and Simulation Technologies Conference*, article 4584, <a href="https://doi.org/10.2514/6.2000-4584">https://doi.org/10.2514/6.2000-4584</a>

Fransos, D & Bruno, L 2006, 'Determination of the aeroelastic transfer functions for streamlined bodies by means of a Navier–Stokes solver', *Mathematical and Computer Modelling*, vol. 43, no. 5–6, pp. 506–529, <a href="https://doi.org/10.1016/j.mcm.2005.10.002">https://doi.org/10.1016/j.mcm.2005.10.002</a>

Gold, P & Karpel, M 2008, 'Reduced-size aeroservoelastic modeling and limit-cycle-oscillation simulations with structurally nonlinear actuators', *Journal of Aircraft*, vol. 45, no. 2, pp. 471–477, <a href="https://doi.org/10.2514/1.28933">https://doi.org/10.2514/1.28933</a>

Green, MA & Smits, AJ 2008, 'Effects of three-dimensionality on thrust production by a pitching panel', *Journal of Fluid Mechanics*, vol. 615, pp. 211–220, <a href="https://doi.org/10.1017/s0022112008003583">https://doi.org/10.1017/s0022112008003583</a>

Green, WE & Oh, PY 2005, 'A MAV that flies like an airplane and hovers like a helicopter', *In:* Proceedings of the 2005 IEEE/ASME International Conference on Advanced Intelligent Mechatronics, pp. 693–698, <a href="https://doi.org/10.1109/aim.2005.1511063">https://doi.org/10.1109/aim.2005.1511063</a>

Green, WE & Oh, PY 2009, 'A hybrid MAV for ingress and egress of urban environments', *IEEE Transactions on Robotics*, vol. 25, no. 2, pp. 253–263, <a href="https://doi.org/10.1109/tro.2009.2014501">https://doi.org/10.1109/tro.2009.2014501</a>

Hodges, DH & Pierce, GA. 2011, *Introduction to structural dynamics and aeroelasticity,* (2nd ed.). Cambridge University Press

Johnson, B & Lind, R 2009, 'High angle-of-attack flight dynamics of small UAVs', *In:* 47th AIAA Aerospace Sciences Meeting Including the New Horizons Forum and Aerospace Exposition, article 61, <a href="https://doi.org/10.2514/6.2009-61">https://doi.org/10.2514/6.2009-61</a>

Kakade, N, Mani, A, Bhatkar, C, Chaudhari, P & Roshan, R 2023, 'A study on modification of boiler chimney against fouling to enhance the efficiency of boiler', *International Journal of Technology*, vol. 13, no. 1, pp. 22–24, <a href="https://doi.org/10.52711/2231-3915.2023.00003">https://doi.org/10.52711/2231-3915.2023.00003</a>

Kaplan, SM, Altman, A & Ol, M 2007, 'Wake vorticity measurements for low aspect ratio wings at low Reynolds number', *Journal of Aircraft*, vol. 44, no. 1, pp. 241-251, <a href="https://doi.org/10.2514/1.23096">https://doi.org/10.2514/1.23096</a>

Klein, V & Morelli, E 2006, *Aircraft system identification: Theory and practice*, VA: Sunflyte Enterprises, <a href="https://doi.org/10.2514/4.861505">https://doi.org/10.2514/4.861505</a>

Kubo, D 2006, 'Study on design and transitional flight of tail-sitting VTOL UAV', *In:* Proceedings of 25th Congress of ICAS, article 12

Kumar, BKS, Singh, BKJ, Niranjan, BK & Gupta, R 2024, 'Robotics is a: Boon or disguise', *International Journal of Technology*, vol. 14, no. 2, pp. 139–140, <a href="https://doi.org/10.52711/2231-3915.2024.00020">https://doi.org/10.52711/2231-3915.2024.00020</a>

Kurtulus, DF 2019, 'Unsteady aerodynamics of a pitching NACA 0012 airfoil at low Reynolds number', *International Journal of Micro Air Vehicles*, vol. 11, <a href="https://doi.org/10.1177/1756829319890609">https://doi.org/10.1177/1756829319890609</a>

Leishman, GJ 2006, Principles of helicopter aerodynamics with CD extra, Cambridge University Press

Leishman, JG, Bhagwat, MJ & Ananthan, S 2002, 'Free-vortex wake predictions of the vortex ring state for single-rotor and multi-rotor configurations', *In:* AHS International, 58th Annual Forum Proceedings, pp. 642–671

Majid, T & Jo, BW 2021, 'Comparative aerodynamic performance analysis of camber morphing and conventional airfoils', *Applied Sciences*, vol. 11, no. 22, article 10663, <a href="https://doi.org/10.3390/app112210663">https://doi.org/10.3390/app112210663</a> Molaa, AA & Abdulwahid, MA 2024, 'Numerical and experimental study of the impact on aerodynamic characteristics of the NACA0012 airfoil', *Open Engineering*, vol. 14, no. 1, article 20220506, <a href="https://doi.org/10.1515/eng-2022-0506">https://doi.org/10.1515/eng-2022-0506</a>

Mor, M & Livne, E 2005, 'Minimum-state unsteady aerodynamics for aeroservoelastic configuration shape optimization of flight vehicles', *AIAA Journal*, vol. 43, no. 11, pp. 2299–2308, <a href="https://doi.org/10.2514/1.10005">https://doi.org/10.2514/1.10005</a>

Mubassira, S, Muna, FI & Inam, MI 2021, 'Numerical investigation of aerodynamic characteristics of NACA 4312 airfoil with Gurney flap', *Journal of Engineering Advancements*, vol. 2, no. 2, pp. 63-70, <a href="https://doi.org/10.38032/jea.2021.02.001">https://doi.org/10.38032/jea.2021.02.001</a>

Murman, SM 2007, 'Reduced-frequency approach for calculating dynamic derivatives', *AIAA Journal*, vol. 45, no. 6, pp. 1161–1168, <a href="https://doi.org/10.2514/6.2005-840">https://doi.org/10.2514/6.2005-840</a>

Ol, M, McAuliffe, B, Hanff, E, Scholz, U & Raffel, M 2005, 'Comparison of laminar separation bubble measurements on a low Reynolds number airfoil in three facilities', *In:* 35th AIAA Fluid Dynamics Conference and Exhibit, article 5149, <a href="https://doi.org/10.2514/6.2005-5149">https://doi.org/10.2514/6.2005-5149</a>

Patel, AB, Gol, AM, Vyas, AJ, Patel, AI, Dudhrejiya, AV & Chotaliya, UJ 2023, 'A brief review on PET – Polyethylene terephthalate containers', *International Journal of Technology*, vol. 13, no. 1, pp. 50–56, <a href="https://doi.org/10.52711/2231-3915.2023.00006">https://doi.org/10.52711/2231-3915.2023.00006</a>

Pelletier, A & Mueller, TJ 2000, 'Low Reynolds number aerodynamics of low-aspect-ratio, thin/flat/cambered-plate wings', *Journal of Aircraft*, vol. 37, no. 5, pp. 825–832, <a href="https://doi.org/10.2514/2.2676">https://doi.org/10.2514/2.2676</a>

Punekar, S, Sahu, S, Kumar, A & Agrawal, A 2023, 'Study of fish markets and their pattern of Raipur City', *International Journal of Technology*, vol. 13, no. 1, pp. 35–40, <a href="https://doi.org/10.52711/2231-3915.2023.00004">https://doi.org/10.52711/2231-3915.2023.00004</a>

Ronch, A Da, Vallespin, D, Ghoreyshi, M and Badcock, KJ 2012, 'Evaluation of dynamic derivatives using computational fluid dynamics', *AIAA Journal*, vol. 50, no. 2, pp. 470–484, <a href="https://doi.org/10.2514/1.j051304">https://doi.org/10.2514/1.j051304</a>

Roy, S, Moreau, A & Grosbois, M 2007, 'Modeling and simulation of a forward-swept wing, vertical takeoff or landing & thrust vectored remotely piloted vehicle', *In:* Proceedings of the Canadian Aeronautics and Space Institute Annual General Meeting on Aircraft Design and Development Symposium

Salmon, F & Chatellier, L 2022, '3D fluid-structure interaction simulation of a hydrofoil at low Reynolds number', *Journal of Fluids and Structures*, vol. 111, article 103573. <a href="https://doi.org/10.1016/j.jfluidstructs.2022.103573">https://doi.org/10.1016/j.jfluidstructs.2022.103573</a>

Selig, M 2010, 'Modeling full-envelope aerodynamics of small UAVs in realtime', *In:* AIAA Atmospheric Flight Mechanics Conference, article 7635, <a href="https://doi.org/10.2514/6.2010-7635">https://doi.org/10.2514/6.2010-7635</a>

Sharma, P, Kumari, A, Shivali & Sharma, V 2024, 'Impact of food and health in 21st century era: A global economic crises', *International Journal of Technology*, vol. 14, no. 2, pp. 111–114, <a href="https://doi.org/10.52711/2231-3915.2024.00016">https://doi.org/10.52711/2231-3915.2024.00016</a>

Silva, WA & Bartels, RE 2004, 'Development of reduced-order models for aeroelastic analysis and flutter prediction using the CFL3Dv6.0 code', *Journal of Fluids and Structures*, vol. 19, no. 6, pp. 729–745, <a href="https://doi.org/10.1016/j.jfluidstructs.2004.03.004">https://doi.org/10.1016/j.jfluidstructs.2004.03.004</a>

Sitaraman, J & Baeder, JD 2004, 'Computational-fluid-dynamics-based enhanced indicial aerodynamic models', *Journal of Aircraft*, vol. 41, no. 4, pp. 798–810, <a href="https://doi.org/10.2514/1.12419">https://doi.org/10.2514/1.12419</a>

Somashekar, V & Raj, ISA 2021, 'Comparative study on the prediction of aerodynamic characteristics of mini-unmanned aerial vehicle with turbulence models', *International Journal of Aviation, Aeronautics, and Aerospace*, vol. 8, no. 1, article 7, <a href="https://doi.org/10.15394/ijaaa.2021.1559">https://doi.org/10.15394/ijaaa.2021.1559</a>

Song, J, Zhao, K & Liu, Y 2023, 'Survey on mission planning of multiple unmanned aerial vehicles', *Aerospace*, vol. 10, no. 3, article 208, <a href="https://doi.org/10.3390/aerospace10030208">https://doi.org/10.3390/aerospace10030208</a>

Swischuk, R, Mainini, L, Peherstorfer, B, & Willcox, K 2020, 'Projection-based model reduction: Formulations for physics-based machine learning', *Computers & Fluids*, vol. 199, article 104434. https://doi.org/10.1016/j.compfluid.2019.104434

Taira, K & Colonius, T 2009a, 'Effect of tip vortices in low-Reynolds-number poststall flow control', *AIAA Journal*, vol. 47, no. 3, pp. 749–756, <a href="https://doi.org/10.2514/1.40615">https://doi.org/10.2514/1.40615</a>

Taira, K & Colonius, T 2009b, 'Three-dimensional flows around low-aspect-ratio flat-plate wings at low Reynolds numbers', *Journal of Fluid Mechanics*, vol. 623, pp. 187–207, https://doi.org/10.1017/s0022112008005314

Wagner, H 2006, 'Über die Entstehung des dynamischen Auftriebs von Tragflächen', *ZAMM – Journal of Applied Mathematics and Mechanics*, vol. 5, pp. 17-35, <a href="https://doi.org/10.1002/zamm.19250050103">https://doi.org/10.1002/zamm.19250050103</a>

Zhang, M & Graham, JMR. 2020, A computational study of the aeroelastic response of a streamlined bridge deck using large-eddy simulation. Journal of Wind Engineering and Industrial Aerodynamics, 206, 104368. <a href="https://doi.org/10.1016/j.jweia.2020.104368">https://doi.org/10.1016/j.jweia.2020.104368</a>

Zhang, S, Lin, Z, Gao, Z, Miao, S, Li, J, Zeng, L & Pan, D 2024, 'Wind tunnel experiment and numerical simulation of secondary flow systems on a supersonic wing', *Aerospace*, vol. 11, no. 8, article 618, <a href="https://doi.org/10.3390/aerospace11080618">https://doi.org/10.3390/aerospace11080618</a>